THE JOURNAL OF PHYSICAL CHEMISTRY A
A JOURNAL OF THE AMERICAN CHEMICAL SOCIETY

pubs.acs.org/JPCA Article

Product Detection of the CH($X^2\Pi$) Radical Reaction with Cyclopentadiene: A Novel Route to Benzene

Kacee L. Caster, Talitha M. Selby, David L. Osborn, Sebastien D. Le Picard, and Fabien Goulay*

Cite This: *J. Phys. Chem. A* 2021, 125, 6927–6939 Read Online

ACCESS | Metrics & More | Article Recommendations | Supporting Information

ABSTRACT: The reaction of the methylidyne radical (CH($X^2\Pi$)) with cyclopentadiene (c-C_5H_6) is studied in the gas phase at 4 Torr and 373 K using a multiplexed photoionization mass spectrometer. Under multiple collision conditions, the dominant product channel observed is the formation of C_6H_6 + H. Fitting the photoionization spectrum using reference spectra allows for isomeric resolution of C_6H_6 isomers, where benzene is the largest contributor with a relative branching fraction of 90 (±5)%. Several other C_6H_6 isomers are found to have smaller contributions, including fulvene with a branching fraction of 8 (±5)%. Master Equation calculations for four different entrance channels on the C_6H_7 potential energy surface are performed to explore the competition between CH cycloaddition to a C=C bond vs CH insertion into C−H bonds of cyclopentadiene. Previous studies on CH addition to unsaturated hydrocarbons show little evidence for the C−H insertion pathway. The present computed branching fractions support benzene as the sole cyclic product from CH cycloaddition, whereas fulvene is the dominant product from two of the three pathways for CH insertion into the C−H bonds of cyclopentadiene. The combination of experiment with Master Equation calculations implies that insertion must account for ∼10 (±5)% of the overall CH + cyclopentadiene mechanism.

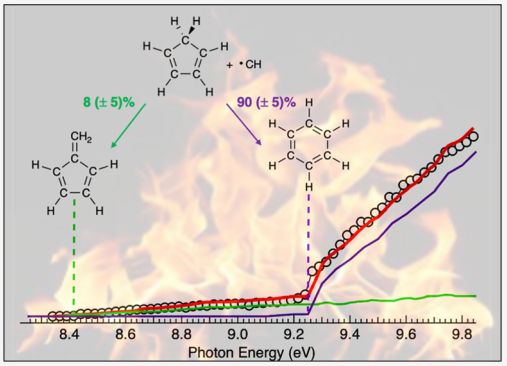

1. INTRODUCTION

The formation of benzene (C_6H_6) in carbon-rich gas phase environments, such as planetary atmospheres,[1,2] the interstellar medium (ISM),[3−6] and combustion processes,[7−9] has long been of interest in many theoretical and experimental studies. Owing to its overall high stability and resistance to oxidation, benzene is regarded as one of the key intermediates in larger carbon molecule growth schemes, and its formation is believed to be a rate-limiting step in this process.[10−12] Through repetitive mechanisms, such as hydrogen-abstraction-C_2H_2-addition (HACA),[13] hydrogen-abstraction-methyl-addition (HAMA),[14] or clustering of hydrocarbons by radical-chain reactions (CHRCR),[15] sequential addition of small aliphatic structures to the first ring can lead to the formation of larger polycyclic aromatic hydrocarbons (PAHs). PAHs are widely abundant in combustion processes, and there is also evidence to suggest their presence and role in the evolution of the interstellar medium.[5,16−20] Once formed, PAHs can aggregate to ultimately form much larger nanoparticle structures, such as soot or carbonaceous dust particles. The efficacy of models that aim to predict and reproduce the composition of combustion and interstellar environments is still limited by an understanding of how benzene and other first-ring structures are formed in the gas phase.[21]

Benzene formation is typically modeled through the reactions of resonantly stabilized radicals, such as propargyl (C_3H_3), allyl (C_3H_5), butadienyl (i-C_4H_5), and cyclopentadienyl (c-C_5H_5, CPD).[22−25] The self-recombination of the propargyl radical is the most familiar route to benzene formation in combustion environments and has been extensively studied through theory and experiment.[10,26−29] Experimental studies in 1,3-butadiene ($H_2CCHCHCH_2$) flames indicate that the i-C_4H_5 + C_2H_2 reaction may also compete with propargyl recombination in benzene formation.[30] To a lesser extent, benzene may also be formed by the cross-recombination of the propargyl and allyl radicals.[22,31] The dominant benzene formation mechanism is likely to depend on the relative concentration of the propargyl radical and therefore on the chemical composition of the environments.[32,33] In addition, for reactions involving self- or cross-recombination of resonantly stabilized radicals, the final product distribution will be very sensitive to the temperature and pressure of the environment.[34] In the interstellar medium, at low temperatures and number densities, stabilization of the initially formed reaction adduct is very improbable, and benzene is more likely to be formed by addition of carbon-centered radicals to a closed-shell molecule. This mechanism allows stabilization in low-pressure environments by loss of H

Received: April 19, 2021
Revised: July 23, 2021
Published: August 10, 2021

https://doi.org/10.1021/acs.jpca.1c03517
J. Phys. Chem. A 2021, 125, 6927−6939

or another free radical fragment. Jones et al.[3] proposed the C_2H + butadiene ($H_2CCHCHCH_2$) reaction as a possible benzene source at low temperatures based on analyses of molecular scattering data obtained in crossed-molecular beam experiments. These results remain to be reconciled with the direct detection of mainly fulvene (c-C_5H_4=CH_2) + H, following the 248 nm photolysis of a C_2HBr + butadiene mixture at room temperature and 4 Torr under multiple collision conditions using multiplexed photoionization mass spectrometry techniques, performed by Lockyear et al.[35] A better understanding of benzene formation in carbon-rich environments requires a systematic investigation of all possible benzene-forming reactions involving a range of open- and closed-shell intermediates.

The highly reactive methylidyne radical (CH) plays a significant role in carbon-rich environments and its reaction with a series of relevant hydrocarbon species has been extensively studied.[36−41] It was one of the first radicals detected in the interstellar medium,[42] and is also believed to play a role in planetary atmospheres where methane is abundant, such as in Saturn's moon, Titan.[43] The CH radical can also form during the pyrolysis of hydrocarbon fuels and other combustion processes and is mostly removed through reactions with abundant fuel molecules.[44−46] The unique structure of the CH($X^2\prod$) radical, which contains a vacant nonbonding molecular orbital in addition to a half-filled π orbital, enables direct addition to C=C double bonds in unsaturated hydrocarbons with little evidence for radical insertion into C−H bonds.[47−50] The intermediate is often short-lived and can undergo isomerization followed by H atom elimination.[40] This mechanism allows for growth in carbon-containing molecules, as described in a general scheme: CH + $C_nH_m \rightarrow C_{n+1}H_m$ + H.[50] A previous study of the CH radical reaction with acetylene has also revealed a competitive molecular hydrogen loss pathway, as described in a general scheme: CH + $C_nH_m \rightarrow C_nH_{m-1}$ + CH_2.[51,52] For reactions with cyclic molecules, such mechanisms may lead to a growth of the ring structures.

The reaction of the CH radical with conjugated cyclic molecules is thought to mostly proceed through cycloaddition onto the unsaturated carbon bonds to form a ringed intermediate. In the case of the reactions with ethyl-substituted furan molecules,[53,54] the initially formed intermediate is found to isomerize through ring opening to form mostly noncyclic final products. However, for the reaction with pyrrole (C_4H_4NH), Soorkia et al.[55] identified the six-membered ring, pyridine (C_5H_5N), as the sole contributing isomer to the product channel, supporting ring expansion through CH cycloaddition. Based upon the evidence from CH + pyrrole, the reaction of CH radical with cyclopentadiene (c-C_5H_6, CPD) could follow a similar ring expansion mechanism. With the identification of cyclopentadiene in the pyrolysis of several conventional fuels,[56−60] the CH + cyclopentadiene reaction may be a route to benzene in combustion environments and other carbon-rich media.

An experimental kinetic investigation of the CH + cyclopentadiene reaction was recently reported by Caster et al.[61] The rate coefficient for the reaction was determined using pulsed laser photolysis (PLP)/laser-induced fluorescence (LIF) techniques and reported as 2.70 ($\pm$1.34) × 10^{-10} cm^3 s^{-1} at 298 K and 5.3 Torr. In addition to the kinetic study, stationary points on the C_6H_7 potential energy surface (PES) including CH cycloaddition and insertion entrance channels were calculated. The fast, experimentally determined rate coefficient is consistent with barrierless entrance channels. In addition, the lack of pressure dependence in the rate coefficient over the 2.7−9.7 Torr range agrees with the mechanism of fast isomerization/decomposition of the initially formed C_6H_7 intermediates. Although no experimental evidence could be gathered about the products from the study, three possible C_6H_6 isomers were discussed: benzene, fulvene, and a bicyclic product, bicyclo[3.1.0]hexa-1,3-diene. Based upon previous product detection studies involving CH radical reactions, it is likely that the cycloaddition entrance channel will dominate the reaction mechanism, offering a direct route to benzene formation.[47,52,55,62] Insertion of the CH radical into one of the three C−H bonds of CPD may be a path to fulvene formation.

The present study provides time- and isomer-resolved detection of products in the CH($X^2\Pi$) + c-C_5H_6 reaction and investigates a mechanism for the formation of benzene and other C_6H_6 isomers from this reaction. Experiments are performed at the Advanced Light Source (ALS) synchrotron at the Lawrence Berkeley National Laboratory (LBNL). Products are sampled from a flow reactor at 4 Torr and 373 K and detected using tunable vacuum ultraviolet (VUV) photoionization coupled to time-of-flight mass spectrometry (TOF-MS). The isomers of the C_6H_6 + H product channel are quantified by fitting the resulting photoionization spectra to experimental reference and simulated photoionization spectra. Master Equation (ME) analysis using the Master Equation Solver for Multi-Energy Well Reactions (MESMER)[63] code is used to predict the cyclic product branching fractions from both the C=C cycloaddition and C−H insertion entrance channels, over a wider range of temperatures (300−1000 K) and pressures (5−760 Torr). Finally, the relative contribution of the cycloaddition and insertion entrance channels to the final product distribution is discussed.

2. EXPERIMENTAL PROCEDURE

The experimental apparatus has been described in detail elsewhere,[52,64,65] and only an abbreviated description is presented here. The CH radical precursor bromoform ($CHBr_3$) in an excess of helium buffer gas flows through a 62 cm slow-flow quartz reaction tube with a 1.05 cm inner diameter. Conditions in the flow tube are held at 4 Torr and at 373 K with a total gas flow rate of 100 sccm such that the total number density is approximately 1.0 × 10^{17} cm^{-3}. The reaction tube is heated to 373 K to avoid deposition of the bromoform precursor on the walls. Multiple data sets using the photolysis laser with CPD with and without $CHBr_3$ were also collected at 298 K. A superposition of the m/z 78 photoion spectra collected at 298 and 373 K can be seen in Figure S2. Due to the bromoform deposition on the reaction tube at 298 K, the 373 K data is chosen to represent the title reaction here, although the same results are obtained at 298 K. Additionally, experiments on the reaction of CPD + deuterated bromoform ($CDBr_3$) were performed at 298 K.

Gas composition and molar flow rates are regulated by mass flow controllers, whereas pressure in the flow tube is regulated by a feedback-controlled butterfly valve throttling a Roots pump that evacuates the flow tube. An unfocused 248 nm KrF excimer laser at 4 Hz repetition rate with laser fluence of ~50 mJ cm^{-2} propagates down the length of the flow tube to generate a uniform concentration of CH radicals from bromoform photolysis (CD radicals from deuterated bromoform) and initiates the reaction of interest.[41] The flow velocity

https://doi.org/10.1021/acs.jpca.1c03517
J. Phys. Chem. A 2021, 125, 6927−6939

is set at ~5 m s^{-1} to replenish the gas mixture between each laser pulse. The gas mixture is sampled about halfway down the length of the flow tube through a 650-μm diameter pinhole. The resulting molecular beam is skimmed via a 0.15 cm diameter skimmer and then ionized by tunable VUV synchrotron radiation. A 50 kHz orthogonal-acceleration time-of-flight mass spectrometer is used to monitor the resulting ions in relation to the excimer laser pulse. The resulting time-resolved mass spectra are normalized for variations in the VUV photon flux, which is continuously monitored via a photodiode placed after the ionization point.

Bromoform, deuterated bromoform, and CPD are introduced in small amounts relative to the helium buffer gas, which comprises the majority of the total flow. A small fraction (15%) of nitrogen is added to sufficiently quench any vibrationally excited CH resulting from the photolysis of the bromoform precursor.[66] Liquid bromoform is held in a glass bubbler at a temperature of approximately 10.0 °C and pressure of 600 Torr and its vapor is carried into the main carrier gas flow by a controlled amount of helium flow such that the density of bromoform in the flow is 2.0 × 10^{13} cm^{-3}. The photodissociation of bromoform is known to occur through successive absorption of photons at 248 nm and can also form $CHBr_2$, CHBr, Br, and Br_2 species in addition to the radical of interest.[67] Based on the CH production efficiency calculated by Romanzin et al.[67] at 248 nm and 44 mJ cm^{-2}, the initial CH number density in the reaction flow is on the order of ~10^{-10} cm^{-3}. The sample of deuterated bromoform ($CDBr_3$) is introduced to the flow in the same manner and conditions.

CPD reagent is prepared through the thermal cracking of dicyclopentadiene ($C_{10}H_{12}$), where the distillate is collected in a liquid nitrogen trap and then vacuum transferred into a 3.79 L stainless steel cylinder. A detailed description of the cyclopentadiene synthesis has been given previously.[61,68] Helium buffer gas was added so that the total pressure was approximately 2023 Torr and the final mixture contained 4.67% CPD. The resulting number density of CPD in the reaction flow tube was approximately 4.8 × 10^{13} molecules cm^{-3}. A mass spectrum was recorded without the 248 nm photolysis laser to validate the presence of CPD and impurities in the prepared gas mixture. Miniscule amounts of m/z 68, 80, and 132 were noted in the mass spectrum of the prepared gas mixture. The 132 amu signal likely represents a small amount of dicyclopentadiene precursor. The relative intensities of these peaks compared to that of the m/z 66 peak suggest that CPD comprises >99% of the molar hydrocarbon flow from this cylinder.

3. COMPUTATIONAL METHODS

The CBS-QB3 method was used to calculate the adiabatic ionization energy of the species of interest.[69] Electronic structure calculations were completed in the Gaussian 09 (G09) suite of programs with the B3LYP/CBSB7 method to optimize the geometry of neutral and cationic structures.[70,71] The PESCAL program was used to calculate the Franck–Condon factors for ionization of each species where experimental photoionization spectra are not available.[72] The PESCAL program performs the calculations within a harmonic approximation and includes the Duschinsky rotation effect for all totally symmetric modes. To obtain the relative photoion spectra for each species, the resulting calculated photoelectron spectra are integrated over the electron binding energy. The calculated photoion spectra do not include contributions from excited cation states nor autoionizing resonances. The photoion spectra are scaled at 11.8 eV to the estimated value of the absolute ionization cross section, per the semiempirical method of Bobeldijk et al.,[73] with an estimated accuracy of ±20% for the cross sections reported. A collection of all of the photoion spectra, calculated and experimental, are shown in Figure S1.

Portions of the C_6H_7 potential energy surface of Senosiain and Miller[24] have been previously calculated using density functional theory (DFT) and CBS-QB3 methods.[61] Additional stationary points are calculated here. Single-point energies for all stationary points were obtained using CBS-QB3. The resulting stationary points are characterized as either local minima or first-order saddle points based upon analysis of their vibrational frequencies. Transition states are found by scanning the bong lengths between intermediates using B3LYP/6-31G(d) and/or through QST3 methods. The presence of a single imaginary frequency confirms the presence of a transition state structure. Intrinsic reaction coordinate calculations on the transition states at the B3LYP/6-31G(d) level of theory confirm their connectivity to the corresponding intermediate structures.

3.1. Master Equation. Branching fractions for the products of the CH($X^2\Pi$) + CPD reaction are calculated using the open-source Master Equation Solver for Multi-Energy Well Reactions (MESMER). Given stationary points of the potential energy surface (PES), MESMER solves coupled differential equations describing the reaction and energy transfer kinetics. The methodology has been described in detail by Glowacki et al.[63] and has been employed to investigate OH radical reactions with unsaturated hydrocarbons as well as CH radical reaction with ammonia.[74,75]

Unimolecular rates for isomerization and decomposition of the reaction intermediates along the PES are calculated using Rice–Ramsperger–Kassel–Marcus (RRKM) theory. Energy transfer processes between intermediates and the buffer gas are modeled using a constant average energy transferred, ΔE_{down} (Table 1). The classical rotor approximation is used for all intermediates as suggested by Pakhira et al.[76] for molecules with rotational constants well below 1 cm^{-1}. The energy grain size typically used for the modeling is 50 cm^{-1}, while a larger grain size of 100 cm^{-1} is used for the sensitivity analysis. The energy transfer and Lennard-Jones parameters (ε, σ) are taken from previous work on CH and OH reactions with unsaturated hydrocarbon and are displayed in Table 1.[75,76]

Table 1. Master Equation Parameters and Their Associated Scanning Range Significant to the MESMER Calculations

	ΔE_{down} (cm^{-1})	ε (cm^{-1})	σ (Å)
intermediates	250 (100–800)	380 (300–600)	4.3 (2–6)
products	250 (100–800)		
argon		11.4	3.47
nitrogen (N_2)		48	3.9

4. EXPERIMENTAL RESULTS

The products of the CH + CPD reaction are studied at 373 K and 4 Torr using multiplexed photoionization mass spectrometry coupled to tunable VUV synchrotron radiation. The photon energy for each data set is scanned over the 8.3–9.8 eV energy range in 25 meV energy steps. Photoionization spectra

https://doi.org/10.1021/acs.jpca.1c03517
J. Phys. Chem. A 2021, 125, 6927–6939

are recorded by averaging at least 500 laser shots at each energy step over a kinetic time range of 0−80 ms relative to the laser pulse. The setup allows for collection of data sets in three dimensions: cation intensity vs mass-to-charge ratio (m/z), kinetic time (t), and photon energy (E). The data are baseline subtracted for prephotolysis signals using the 20 ms time range before each laser pulse and normalized for the VUV photon energies. Plotting the data in two-dimensional (2-D) data sets provides mass spectra that are resolved for either photon energy or kinetic time. Positive ion signals in the mass spectra indicate species created during and after the laser pulse, whereas negative ion signals indicate species that are depleted due to the laser pulse. Photoionization spectra are obtained by taking a one-dimensional (1-D) slice over the mass species of interest from the 2-D energy-resolved mass spectra. The photoionization spectra enable identification of different isomers appearing at a single mass of interest through fitting of each observed spectrum with the reference spectra of individual isomeric components. Experimental photoionization spectra of pure isomers are available for two species, benzene[77] and fulvene,[35] and are utilized as basis functions in the fit. For isomers without an experimental spectrum, the photoionization spectra are predicted from the integral of calculated Franck−Condon factors, assuming that direct ionization dominates. A linear least-squares fit of a set of basis functions to the experimental spectra enables quantification of each isomer if the absolute photoionization cross sections are known.

The experimental photoionization spectra are reported as individual measurements with error bars reported from twice the shot noise in the number of the detected ion counts ($2\sqrt{N}$). Since several data sets were recorded at both 298 and 373 K, the photoionization spectra were superimposed, revealing little to no difference in the overall shape due to the temperature change (see Figure S2).

Under the present experimental conditions, collisional quenching with the He and N_2 buffer gases is expected to rapidly thermalize all of the products to the temperature of the flow. As long as the unimolecular dissociation of the reaction intermediates occurs with a rate higher than the collision rate ($\sim 20 \times 10^6$ s^{-1}), the present branching fractions provide information about the unimolecular isomerization and dissociation scheme of the nascent reaction intermediates as would be observed at very low pressures.

4.1. Cyclopentadiene Photodissociation. Figure 1 displays mass spectra recorded upon photolysis of CPD (a) without and (b) with bromoform. The mass spectra were integrated over the energy range of interest (8.3−9.8 eV) and kinetic time of 0−80 ms. The absorption cross section of CPD was previously reported as 4.5×10^{-18} cm^2 at 248 nm,[78] and the molecule is known to readily photodissociate at this wavelength.[79] The depletion of CPD (m/z 66) is evident in both spectra from the negative signal displayed in the mass spectra. The depletion of the ^{13}C isotopologue of the cyclopentadiene reactant at m/z 67 is also visible in the mass spectra. Although only a portion of the depletion is shown in Figure 1, the intensity ratio of the two masses supports the assignment of m/z 67 as the singly substituted ^{13}C isotopologue.

Analysis of the 248 nm photodissociation of cyclopentadiene allows us to directly account for photoproducts and their secondary reactions. From Figure 1a, two primary products are identified through peaks appearing at m/z 39 and 65. Figure 2

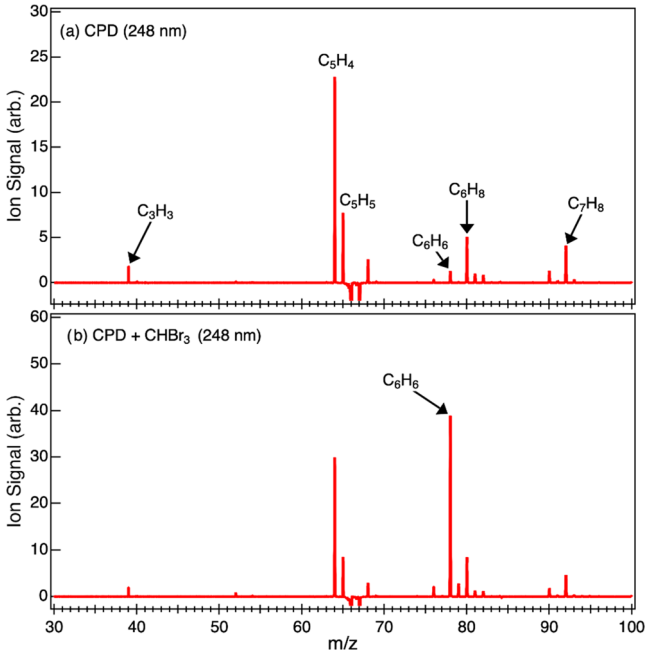

Figure 1. Mass spectra integrated over the 8.3−9.8 eV photon energy and 0−80 ms kinetic time range obtained from (a) photolysis of the CPD (C_5H_6) mixture alone in helium and nitrogen buffer gases and (b) bromoform ($CHBr_3$) and CPD mixture in helium and nitrogen buffer gases at 4 Torr and 373 K. Negative ion signals indicating depleting species are truncated.

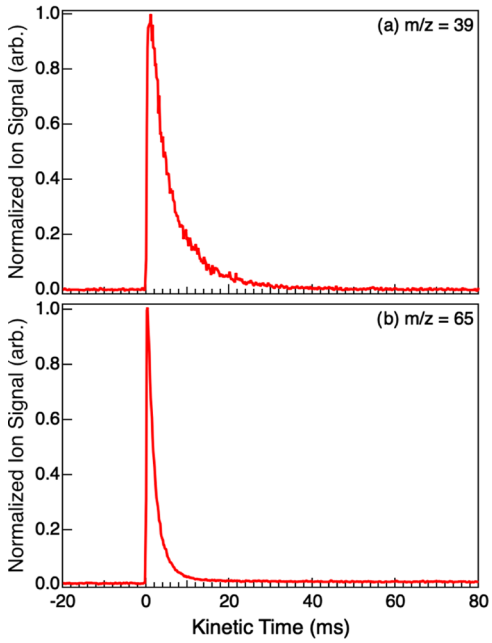

Figure 2. Normalized kinetic traces obtained from cyclopentadiene photolysis at 248 nm at (a) m/z 39 and (b) m/z 65. The ion signal is integrated over the 8.3−9.8 eV energy range.

displays the kinetic traces of (a) m/z 39 and (b) m/z 65. The shapes of the traces in Figure 2 are consistent with the formation of a radical by the laser pulse. The signal at m/z 65 corresponds to the formation of cyclopentadienyl (c-C_5H_5) arising from the H loss channel of cyclopentadiene reactant. Under the experimental conditions, and neglecting other CPD photodissociation pathways, the maximum cyclopentadienyl

https://doi.org/10.1021/acs.jpca.1c03517
J. Phys. Chem. A 2021, 125, 6927−6939

(m/z 65) number density in the flow is ~1×10^{13} cm^{-3}. The formation of cyclopentadienyl is also confirmed by the ionization energy onset of m/z 65 at ~8.4 eV and from reference photoion spectra obtained by Savee et al.[80] and Hansen et al.[81] (see Figure S3). Another prominent peak at m/z 64 suggests the formation of C_5H_4 species, ethynylallene, methyldiacetylene, and pentatetraene, which are identified by fitting their absolute reference spectra to the experimental photoion spectrum (Figure S3).[82] The m/z 64 products are likely to be the result of H_2 loss from the cyclopentadiene reactant and have been previously reported in CPD photolysis studies.[83,84] The shape of the photoionization spectrum of C_5H_4 (m/z 64) in Figure S3 is also noticeable in the experimental m/z 65 spectrum, supporting the assignment of a portion of the m/z 65 signal to the $^{13}CC_4H_4$ isotopologue of m/z 64, formed from CPD photolysis. The resonantly stabilized radical propargyl (C_3H_3) is identified at m/z 39 by its ionization energy onset at ~8.65 eV and through comparison of the recorded photoionization spectrum with reference spectra.[85] The corresponding kinetic time trace in Figure 2a displays a fast increase and a slower decay that is consistent with the formation of a resonantly stabilized radical. The vinyl radical (C_2H_3) is also observed at m/z 27 as a propargyl radical coproduct.[84] The vinyl radical is expected to be much more reactive than the resonantly stabilized propargyl radical and thus accumulate in lower concentrations than those reported for m/z 39. This is supported by a comparatively faster decay time in the m/z 27 kinetic trace, as shown in Figure S4. A small amount of ion signal at m/z 27, corresponding to the vinyl radical (C_2H_3), is observed experimentally but not included in the mass range of Figure 1a due to a comparably low intensity.[86]

Lower intensity peaks are observed at m/z 38, 40, 52, 54, and 63 that are indicative of other cyclopentadiene photodissociation channels or products of fast bimolecular reactions. The photodissociation products further react to form larger mass secondary products, such as those observed at m/z 68, 76, 78, 80, 82, 90, and 92. Further insight into the m/z 78 photoproducts will be provided in Section 4.3.

Through comparison of the CH + CPD mass spectra, shown in Figure 1b, with that of CPD photolysis shown in Figure 1a, it can be seen that the relative intensity of the peaks corresponding to the CPD photoproducts does not significantly change upon addition of bromoform to the flow. The only exception arises in the mass of interest, m/z 78, where the intensity is 18 times greater in the presence of CH radical precursor. This increase in ion signal can be attributed to C_6H_6 neutrals formed in the title reaction: $CH + C_5H_6 \rightarrow C_6H_6 + H$.

4.2. CH + Cyclopentadiene. Photodissociation of bromoform at 248 nm effectively produces the CH($X^2\Pi$) radical through a two-photon process.[41,87] In addition to the radical of interest, it is also known to form $CHBr_2$, CHBr, Br, and Br_2 species, which can subsequently react with other photoproducts and give rise to higher mass signals that may lie outside of the range of the mass spectra in Figure 1b (see Figure S5 for m/z up to 150). The reaction of cyclopentadienyl with molecular bromine results in the appearance of peaks at m/z 144/146. Relatively less intense peaks also appear at m/z 106/108 and 118/120 from vinyl and propargyl radical reactions with atomic Br to form $C_2H_3{}^{79}Br/C_2H_3{}^{81}Br$ and $C_3H_3{}^{79}Br/C_3H_3{}^{81}Br$, respectively (insets in Figure S5). Most of the m/z 106 signal in Figure S5 comes from CPD photoproduct side reactions. Small peaks appear at m/z 93/95, resulting from single-photon 248 nm photolysis of bromoform, confirming the presence of $CH_2{}^{79}Br/CH_2{}^{81}Br$ formed through H atom reactions with CHBr photoproducts. Identification of these photoproducts is further supported by their radical-like temporal profiles and confirms the presence of CHBr singlet carbene species. The small relative intensity of the peaks and temporal profiles at m/z 92/94 indicates very low yields of this photoproduct, which is in agreement with previous studies of 248 nm photolysis of bromoform.[88]

Figure 3 shows the normalized kinetic time trace of the m/z 78 ion signal with the addition of bromoform. The observed

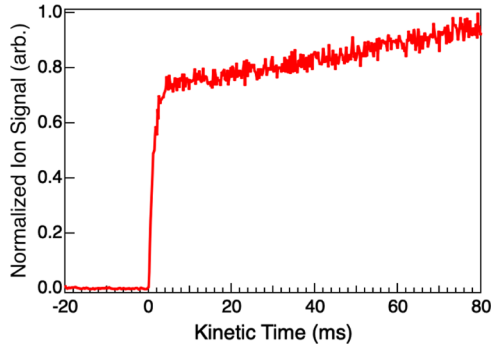

Figure 3. Normalized kinetic trace of m/z 78 obtained by the reaction of CH($X^2\Pi$) radical with cyclopentadiene. The ion signal is integrated over the 8.3−9.8 eV energy range.

increase of the m/z 78 temporal profile has a corresponding k_{1st} value of ~860 s^{-1} observed through exponential fits to the data. The k_{1st} value for the observed increase of photoproduct m/z 65 is ~8700 s^{-1} and is faster in comparison to the k_{1st} value (~450 s^{-1}) for the m/z 78 kinetic trace obtained from the photolysis of CPD alone. Once the m/z 78 products are formed, a slight increase in signal continues over the kinetic time range. This has been observed in a previous CH radical study[52] and can likely be attributed to divergence of the laser beam along the flow tube that leads to a gradient in the initial CH radical number density. A similar trend is observed in the CPD depletion time profile. The contribution of any slower secondary reactions that may also form m/z 78 have been ruled out because the photoionization spectrum of m/z 78 does not change with increasing kinetic time. It is also worth noting that a small peak at m/z 79 appears in the mass spectrum from the title reaction as well, which is consistent with ^{13}C contribution from the C_6H_6 product. The lack of a temporal decay that would be expected for a free radical in the kinetic trace of the m/z 79 product further rules out any contribution from stabilization of a C_6H_7 radical intermediate.

Based on the comparison between the two mass spectra in Figure 1 and the discussion above, formation of m/z 78 through H elimination seems to be the only observed CH + CPD product channel. Since the CPD number density is relatively large in comparison to its photoproducts, it is likely that the CH + CPD reaction is the main route for CH decay and m/z 78 increase. Because of cyclopentadienyl formation by photodissociation of cyclopentadiene, we avoid drawing any conclusions on the contribution from the abstraction channel $CH + C_5H_6 \rightarrow CH_2 + C_5H_5$.

4.3. m/z 78 Isomer Products. Figure 4 shows the m/z 78 photoionization spectra for (a) CPD alone and (b) CPD + $CHBr_3$ at 4 Torr and 373 K. Both spectra are integrated over 0−80 ms after the photolysis pulse and are the result of an

https://doi.org/10.1021/acs.jpca.1c03517
J. Phys. Chem. A 2021, 125, 6927−6939

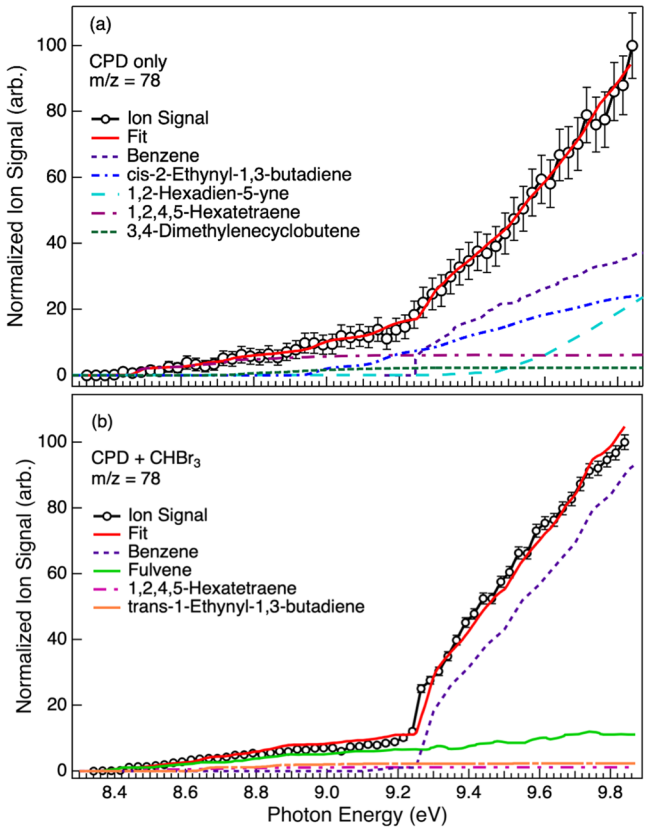

Figure 4. Photoionization spectra of m/z 78 ion signal obtained from (a) 248 nm photolysis of cyclopentadiene and (b) 248 nm photolysis of bromoform (CH radical precursor) and cyclopentadiene reactant integrated over the 0−80 ms time range (open circles) at 4 Torr and 373 K and background subtracted for CPD photolysis. The spectra are shown with error bars calculated from twice the shot noise in the number of detected ion counts ($2\sqrt{N}$). The solid red lines in both panels are a fit to the data using the absolute photoionization spectra of benzene (purple dashed line)[77] and fulvene[35] (solid green line) as well as the integrated photoelectron spectra of six other C_6H_6 isomers: *cis*/*trans*-1-ethynyl-1,3-butadiene (1E13BD) (solid orange line), 1,2,4,5-hexatetraene (1245HT) (magenta dot-dashed line), *cis*-2-ethynyl-1,3-butadiene (2E13BD) (dark blue dot-dashed line), 1,2-hexadien-5-yne (12HD5Y) (light blue dashed line), and 3,4-dimethylenecyclobutene (dark green dashed line). The fitted branching fractions are displayed in Table S1 for (a) and Table 2 for (b).

individual measurement. Each photoion spectrum is reported with error bars calculated from twice the shot noise in the number of detected ion counts ($2\sqrt{N}$). To remove the contribution of C_6H_6 signal that arises only from the C_5H_6 + laser interaction, we subtract the m/z 78 spectrum in Figure 4a from the m/z 78 spectrum obtained when $CHBr_3$ is added to the system (Figure 4b). Both experiments were performed under identical conditions except that an equivalent mass flow of helium is replaced by $CHBr_3$ in the second experiment. The resulting spectrum in Figure 4b should therefore contain only the m/z 78 contributions from the CH + C_5H_6 reaction. The addition of bromoform to the reaction flow increases the sharp onset at 9.25 eV that is characteristic of benzene.[89]

The spectra are fit using a least-squares fitting routine to the weighted sums of absolute photoionization data of several C_6H_6 isomers obtained from previous studies by Lockyear et al.[35] and Cool et al.[77] and calculated here (see Figure S1). The residuals of the fitting routines on the experimental photoionization spectra were within 5% for CPD only (Figure 4a) and within 3% for CPD + $CHBr_3$ (Figure 4b). The selection of the C_6H_6 isomers included in the fit was based upon the ionizing energy range considered here (8.3−9.8 eV) and other reasonable products expected based on previous studies of the C_6H_6 and C_6H_7 potential energy surfaces.[10,24,28,90−92] Based upon this selection criteria, eight possible C_6H_6 isomers were included in the fitted spectrum: benzene, fulvene, *cis*-2-ethynyl-1,3-butadiene (2E13BD), *trans*-1-ethynyl-1,3-butadiene (1E13BD), 1,2,4,5-hexatetraene (1245HT), 1,2-hexadien-5-yne (12HD5Y), 3,4-dimethylcyclobutene (34DMCB), and 1,3-hexadien-5-yne (13HD5Y). Within the energy resolution of the experiment (~40 meV), it is not possible to differentiate between the *trans*- and *cis*-1-ethynyl-1,3-butadiene (1,3-hexadien-5-yne) species. The C_6H_6 isomers along with their structures, CBS-QB3 calculated adiabatic ionization energies, and resulting fitted branching fractions with 2σ standard deviation from Figure 4b are shown in Table 2. Table S1 shows

Table 2. Structures, CBS-QB3 Adiabatic Ionization Energies, and Fitted Product Branching Fractions for the m/z 78 Photoionization Spectrum of CPD + $CHBr_3$ Shown in Figure 4b

C_6H_6 Isomer (Abbreviated Name)	Geometry	$IE_{CBS-QB3}$ (eV)	Branching Fraction (% ± 2σ)
Benzene		9.25	90 (± 5)
Fulvene	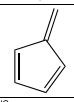	8.36	8 (± 5)
Cis-2-ethynyl-1,3-butadiene (2E13BD)	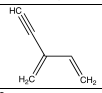	8.93	0 (± 0)
Trans/Cis-1-ethynyl-1,3-butadiene (1E13BD)	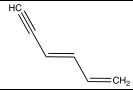	8.62	1 (± 2)
1,2,4,5-Hexatetraene (1245HT)	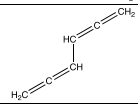	8.49	1 (± 2)
Hexa-1,2-dien-5-yne (12HD5Y)	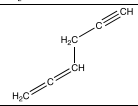	9.30	0 (± 4)
3,4-Dimethylenecyclobutene (34DMCB)	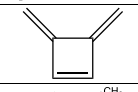	8.76	0 (± 2)
Hexa-1,3-dien-5-yne (13HD5Y)	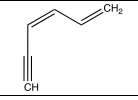	8.64	0 (± 3)

the product distributions for Figure 4a (CPD only). Although the absolute photoionization spectrum of fulvene is not shown in Figure 4a, it was included in the fitting routine with a reported branching fraction of 0 (±7)%, as shown in Table S1.

From the fitting results, benzene is the largest contributing isomer contributing 90 (±5)% to the CPD + CH product distribution. Fulvene, which is not detected in the case of CPD photolysis (Table S1), has a branching fraction of 8 (±5)% and is the only other cyclic isomer assigned. Very minor contributions from 1-ethynyl-1,3-butadiene (1 (±2)%) and

https://doi.org/10.1021/acs.jpca.1c03517
J. Phys. Chem. A 2021, 125, 6927−6939

1,2,4,5-hexatetraene (1 (±2)%) are also reported. Fitting the photoionization spectra to only benzene and fulvene reveals no significant difference (Figure S6). In addition, a minor contribution from another C_6H_6 isomer, 1,5-hexadiyne, cannot be ruled out, but is not included into the experimental fits because its ionization energy onset (9.98 eV) is outside the energy range used here. Previous single-point energy calculations of 1,5-hexadiyne suggest that it is thermodynamically accessible on the C_6H_7 PES.[61] However, it is not anticipated to change the assignment of benzene as the major product in the CPD + CH reaction but rather only play a small role in the minor C_6H_6 product branching fractions. Product detection experiments of CH radical reaction with the cyclopentadiene analog, pyrrole (C_4H_4NH), further suggest that the major product is cyclic in structure.[93]

4.4. CD + Cyclopentadiene. Figure 5 displays the mass spectra recorded upon photolysis of CPD with bromoform

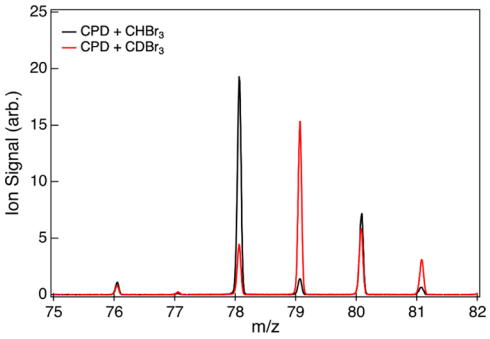

Figure 5. Mass spectra integrated over the 8.3−9.8 eV photon energy and 0−80 ms kinetic time range obtained from photolysis of the bromoform ($CHBr_3$, black line) and CPD mixture in helium and nitrogen buffer gases and deuterated bromoform ($CDBr_3$, red line) and CPD mixture in helium and nitrogen buffer gases at 4 Torr and 298 K.

($CHBr_3$, black line) and with deuterated bromoform ($CDBr_3$, red line). The mass spectra were integrated over the energy range of interest (8.3−9.8 eV) and kinetic time of 0−80 ms at 298 K. Comparison of the CPD + $CDBr_3$ mass spectra (red line) with the CPD + $CHBr_3$ mass spectra (black line) shows a significant increase in m/z 79 signal relative to the m/z 78 signal. In the CD + CPD reaction, a 1:3.3 C_6H_6/C_6H_5D (corrected for ^{13}C) ratio is observed. Figure S7 shows the photoionization spectra for the reaction of $CDBr_3$ + CPD at (a) m/z 78 and (b) m/z 79 with fits to the absolute photoionization spectra of benzene[77] and fulvene.[35] The reported branching fractions for the fits to m/z 78 in Figure S7a are 76 (±2) and 24 (±1)% for benzene and fulvene, respectively. The branching fractions for m/z 79 in Figure S7b are 66 (±2) and 34 (±1)% for benzene and fulvene, respectively. Further insight into the mechanisms behind the formation of C_6H_5D/C_6H_6 species is provided in Section 5.

4.5. H-Assisted Isomerization. It is also necessary to discuss the role that H-assisted isomerization could have in the branching fraction distribution of the C_6H_6 products. Several studies of the C_6H_7 PES reveal that the exit channel barriers are low enough with respect to the C_6H_6 + H products for the process to easily occur.[61,90,91,94] However, under the experimental conditions of this work, there is very little evidence to support that H-assisted isomerization plays a major role in the formation of benzene. The fast increase in the m/z 78 temporal profiles does not indicate the occurrence of H-assisted isomerization in the products. A comparison of the branching fractions extracted from the m/z 78 photoionization spectra integrated over various kinetic time ranges (0−4, 0−10, and 10−80 ms) does not reveal evolution in the product isomer distribution (see Figure S8). In fact, the branching fraction of benzene remains consistent at 90 (±3)% over the 0−4 ms time range in comparison to the 90 (±5)% reported over the 0−80 ms time range. Integrated over longer time ranges (0−10 and 10−80 ms) and within the error bars of the fitting routine, the benzene branching fraction remains unchanged.

5. DISCUSSION

The isomeric distribution of the C_6H_6 + H product channel was determined experimentally using photoionization mass spectrometry between 8.3 and 9.8 eV ionizing energy range at 4 Torr and 373 K. Fits to the photoionization spectrum of the m/z 78 channel reveal benzene as the major product channel with a branching fraction of 90 (±5)%, and fulvene representing 8 (±5)% of the products. The $CDBr_3$ + CPD reaction was also experimentally investigated over the 8.3−9.8 eV ionizing energy range at 4 Torr and 298 K. The reactions of the CH radical are generally believed to follow either a C═C cycloaddition or C−H insertion mechanism.[50] If the subsequent isomerization of the nascent C_6H_6 molecule (unimolecularly or via H-assisted isomerization) is negligible, then the distribution of the detected C_6H_6 isomers reflects the different pathways of the title reaction. In the following sections, we discuss the formation of benzene and fulvene through cycloaddition and C−H insertion using PES and RKKM-ME calculations. Insertion into CPD C−C σ bond is also considered.

5.1. Cycloaddition Mechanism. The C_6H_7 potential energy surface for CH cycloaddition onto a C═C bond of CPD is displayed in Figure 6. This surface has been previously calculated using CBS-QB3 and DFT methods in another publication and is only briefly described here.[61] All intermediates and reaction products were found to be highly exothermic relative to the reactants as shown in Figure 6. Pathways to additional cyclic and linear C_6H_6 products on the C_6H_7 PES have been previously considered in other works[3,24,35,89] and are included in a more extensive C_6H_7 PES in the Supporting Information (Figure S9).

On the CH + CPD PES, the CH may add by cycloaddition to the π system that is delocalized across C2−C3−C4−C5 forming INT1 through a barrierless process. INT1 has three isomeric contributions: addition onto the C2−C3 carbons (forming bicyclic intermediates INT1A and INT1B)[61] and addition onto the C3C4 carbons (forming the tricyclic intermediate INT1C). INT1A and INT1B interconvert across a relatively low-lying TS3. INT1C can lose a H atom to give benzvalene + H (−126.1 kJ mol^{-1}). No barrier was located for this pathway at the CBS-QB3 level. A barrier of a few kJ mol^{-1} to benzvalene + H would only further tighten the transition state compared to a barrierless pathway and raise the energy of the transition state. A much lower energy pathway is isomerization to INT1B via TS3b. As a result, it is most likely that addition at the C3-C4 position effectively leads only to INT1A and INT1B, with isomerization of these intermediates to the more stable INT2 and INT3 species. The PES in Figure 6 includes two additional H-loss channels: INT2 → TS2 → benzene + H (purple) and INT3 → INT4 → TS8 → fulvene +

https://doi.org/10.1021/acs.jpca.1c03517
J. Phys. Chem. A 2021, 125, 6927−6939

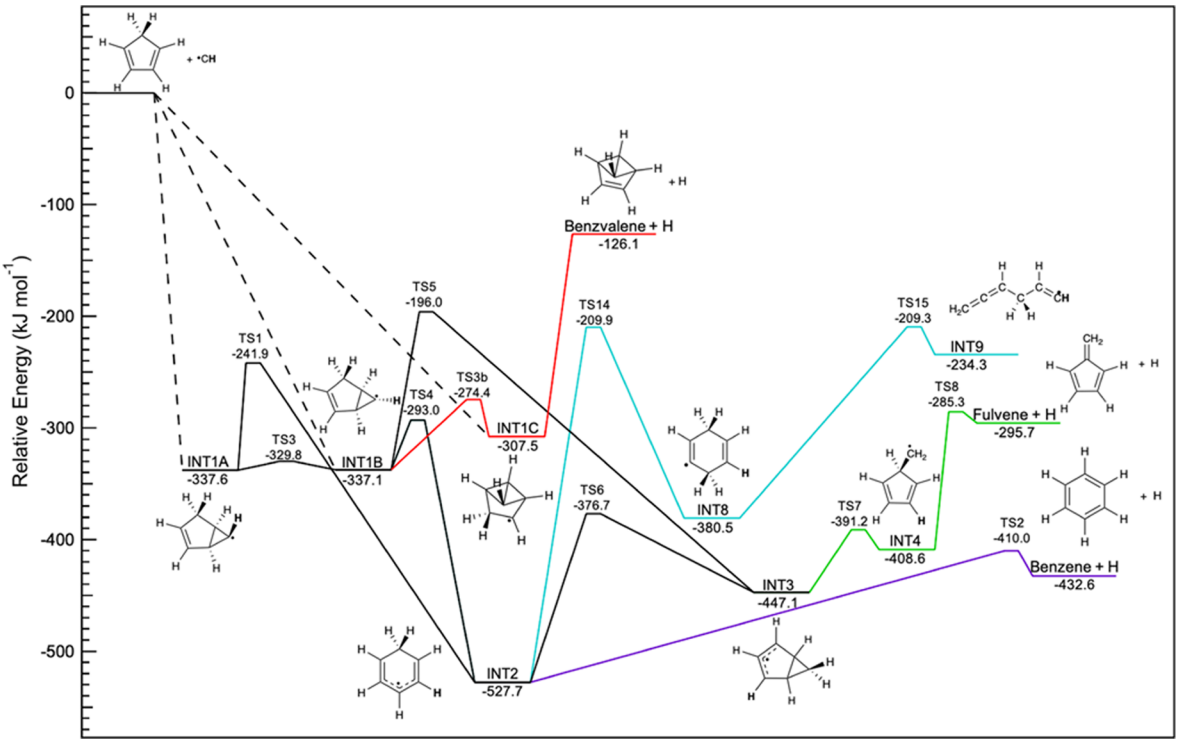

Figure 6. Portion of the CBS-QB3 calculated C_6H_7 potential energy surface proceeding through C**H** cycloaddition across a C═C bond of CPD.[61] The reaction enthalpies (300 K) are given in kJ mol^{-1} for the intermediates and products relative to the reactants. The PES shows those pathways (black, green, and purple) included in the MESMER calculations. The light blue pathway leading to the formation of INT9 and the red pathway to bemzvalene are not included in the MESMER calculations. The hydrogen atom from the CH radical is labeled in bold, assuming formation of INT2.

H (green). An alternate H shift from INT2 can occur through TS14 to form INT8, which can further ring open to form INT9 (light blue). INT9 is the bottleneck intermediate leading to the formation of the other six C_6H_6 products included in the fits to the photoionization spectra of Figure 4. A more extensive C_6H_7 PES that includes pathways from INT9 to the formation of these products is provided in the Supporting Information (Figure S9). A third cyclic H-loss channel,[61] INT3 → bicyclo[3.1.0]hexa-1,3-diene + H, is also depicted in Figure S9.

To better understand the role of the cycloaddition reaction mechanism in the formation of benzene, RRKM-based Master Equation (ME) calculations using the open-source software MESMER have been performed on a portion of the C_6H_7 PES shown in Figure 6. The light blue pathway INT2 → TS14 → INT8 → TS15 → INT9 is not included in the MESMER calculations because the intermediates and transition barriers are expected to be less accessible relative to the pathways leading to the formation of cyclic products, likely due to high energy barriers (ΔE = 317.8 and 171.2 kJ mol^{-1}) and entropic factors due to ring opening. The barrierless formation of the bicyclic product (Figure S9) is omitted as well. The PES used for the MESMER calculations is displayed in Figure S10. In addition, due to the high energy of the H-loss channel from INT1C relative to the transition state for its isomerization to INT1B, the most likely fate of INT1C is isomerization to INT1B, and we omit the H-loss pathway to benzvalene + H. Therefore, in the ME calculation, the reaction is modeled to proceed through CH cycloaddition onto the π system, either yielding INT1A/1B with a rate coefficient set to the experimental one.[61] The reactant number densities are chosen from the experimental conditions. The intermediates INT1A and INT1B are found to be in equilibrium. Two cyclic C_6H_6 products from the PES are considered in the ME analysis: benzene and fulvene. The ME analysis is run for temperatures ranging from 300 to 1000 K and pressures ranging from 5 to 760 Torr in both Ar and N_2 as buffer gas. Benzene is found to be the sole cycloaddition product (>99%) over the considered pressure and temperature ranges. Sensitivity analyses are performed to investigate the effect of model input parameters on the benzene population. The energy transfer parameter (ΔE_{down}) is varied from 100 to 800 cm^{-1} while the Lennard-Jones parameters ε and σ are varied from 300 to 600 cm^{-1} and 2 to 6 Å, respectively, as shown in Table 1. Over these ranges, the final modeled benzene population is found to be independent of temperature and pressure and the initial input parameters.

Figure 7 displays the microcanonical rate constants calculated using RRKM theory for the unimolecular isomerization and dissociation of the reaction intermediates. Following INT1 formation by cycloaddition of the CH radical (INT1A and INT1B are in equilibrium), isomerization occurs very rapidly through ring opening to form INT2. The H-shift pathway that competes with this process, converting INT1 to bicyclic INT3, is calculated to be several orders of magnitude slower than the ring-opening path to INT2 and considered unfavorable relative to expansion to a six-membered ring. Additionally, the isomerization of INT2 to bicyclic INT3 through TS6 (ΔE = 151 kJ mol^{-1}) is relatively slow, being on the same order of magnitude as the INT1B → TS5 → INT3 H-shift pathway (ΔE = 142.1 kJ mol^{-1}). Based on the PES in Figure 6, the formation of fulvene + H through cycloaddition

https://doi.org/10.1021/acs.jpca.1c03517
J. Phys. Chem. A 2021, 125, 6927−6939

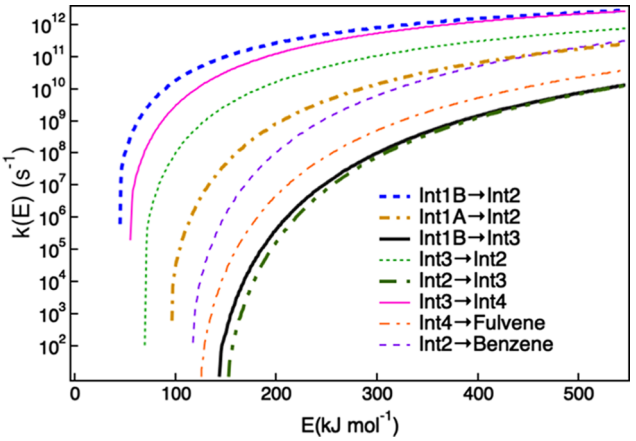

Figure 7. RRKM theory calculated microcanonical rate constants for the unimolecular isomerization and dissociation of the C_6H_7 reaction intermediates. The energy origin is set to INT2.

can only proceed through the three-membered ring opening of the bicyclic INT3 to INT4 followed by H elimination through TS8. Overall, the most important kinetic competition is INT2 → TS6 → INT3 (the rate-limiting step to fulvene formation) vs INT2 → TS2 → benzene. The latter pathway has a substantially larger rate constant at all energies. The microcanonical rates support benzene being the most energetically and entropically favorable cycloaddition product, with no fulvene formation. This comparison between experiment and theory suggests that fulvene is more likely to be formed by barrierless insertion of the CH radical into one of the C−H bonds of CPD.[61]

Previous studies have investigated the role of CH insertion into a C−C σ bond.[95,96] In the case of the reaction with CPD, addition into the C3−C4 σ bond directly forms INT 2. A transition state was unable to be located at the level of theory employed here. According to the RRKM microcanonical rates, this mechanism will predominantly lead to benzene-d_0 + H and benzene-d_1 + H in the case of CD + CPD. It is therefore not possible to discriminate between C═C cycloaddition and C−C addition based on the experimental results and RRKM-ME calculations. However, there is evidence to suggest that C−C addition mechanisms may be sterically hindered for reactions with larger hydrocarbons.[97,98]

5.2. C−H Insertion Mechanism. Figure 8 displays the C_6H_7 potential energy surface for CH insertion into each of the three unique C−H bonds of CPD. This surface has been previously calculated using CBS-QB3 and DFT methods in another publication,[61] although TS12 and TS13 were not previously reported. There are three insertion channels: into the C−H bond of one of the sp^2 carbons to form INT5 or INT7, and into one of the C−H bonds of the sp^3 carbon to form INT4. As discussed previously INT4 may lead to benzene formation through successive ring closing and opening to form INT2 followed by H-loss. INT4 can also directly lose a hydrogen atom to form fulvene through TS8. Alternatively, INT4 can isomerize to INT6 or INT7 through TS9 and TS10, respectively. The insertion intermediates INT5 and INT7 can directly decompose to fulvene + H through TS12 and TS13 or isomerize into each other through TS11.

The theoretical method used here does not allow for calculation of the relative contributions between the cycloaddition and C−H insertion entrance channels nor between the three insertion channels. Nonetheless, RRKM-ME

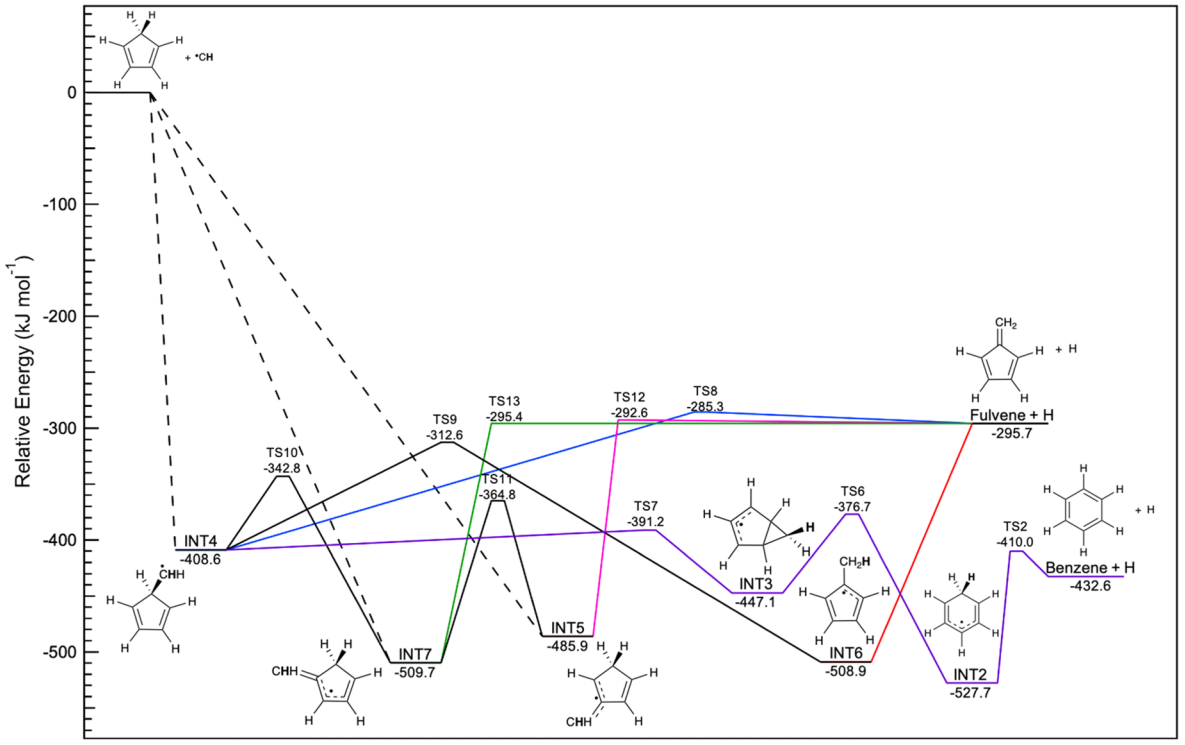

Figure 8. Portion of the CBS-QB3 calculated C_6H_7 potential energy surface proceeding through CH insertion across a C−H bond of CPD.[61] The reaction enthalpies (300 K) are given in kJ mol^{-1} for the intermediates and products relative to the reactants. The hydrogen atom from the CH radical is labeled in bold.

https://doi.org/10.1021/acs.jpca.1c03517
J. Phys. Chem. A 2021, 125, 6927−6939

calculations are performed using the PES in Figure 8, not including INT6. Within the level of theory employed here, there is no identifiable saddle point for decomposition of INT6 into fulvene + H. The PES used in the MESMER calculations is displayed in Figure S10. Three individual calculations are performed starting with direct formation of INT4, INT5, or INT7, respectively. The calculations are performed using the same parameters as for the cycloaddition calculations. At room temperature and 5 Torr, benzene formation is found to be the dominant mechanism (85%) when starting from the formation of INT4. In the case of the direct formation of the insertion intermediates INT5 and INT7, fulvene formation becomes dominant with branching fractions of 82 and 74%, respectively.

Figure 9 displays the calculated fulvene branching fractions for isolated cycloaddition or isolated C−H insertion as a function of temperature upon reaction of the CH radical with CPD to from INT1 (black), INT4 (red), INT5 (green), or INT7 (blue). Considering the maximum fulvene fraction from insertion (82% after formation of INT5), the total branching fraction of the insertion mechanism must represent at least 10 (±5)% of the overall CH + CPD reaction mechanism to reproduce the measured 8 (±5)% fulvene fraction. Assuming that the insertion/cycloaddition fraction does not change with temperature, the overall fulvene/benzene branching fraction from the CH + CPD reaction is only slightly dependent on temperature. Benzene is therefore likely to remain the main cyclic reaction product from the CH + CPD reaction at combustion temperatures with a non-negligible amount of fulvene.

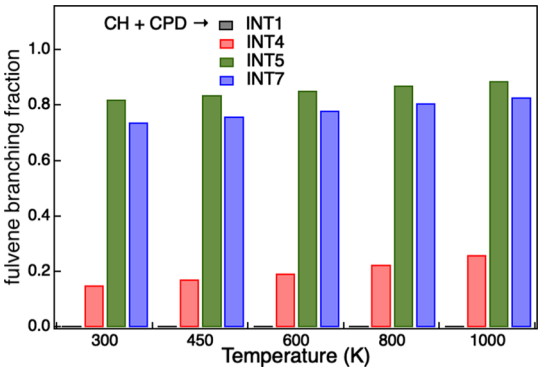

Figure 9. Calculated fulvene branching fractions for CH cycloaddition to INT1 (black) and insertion of the CH radical into one of the C−H bonds of CPD forming INT4 (red), INT5 (green), or INT7 (blue).

The 1:3.3 m/z 78:79 ratio from Figure 5 combined with the benzene to fulvene branching ratios from Figure S6 suggests that the benzene-d_1 + H channel is the main exit channel. This is in agreement with cycloaddition being the dominant mechanism. The benzene-d_0 products can be attributed to the C−H insertion mechanism through formation of INT4 undergoing a ring closure to INT3 following by 1:1 H:D elimination. The formation of both fulvene-d_0/fulvene-d_1 suggests either formation of INT6 and 2:1 H/D elimination or H/D scrambling along the insertion PES. Such hydrogen scrambling is expected for highly exothermic reactions. Overall, the $CDBr_3$ experiments are consistent with cycloaddition as the main reaction pathway with a non-negligible fraction of C−H insertion. Considering the maximum fulvene fraction from insertion in Figure 9 (82% after formation of INT5), as well as the CD + CPD m/z 78:79 ratio from Figure 5, the total branching fraction of the insertion mechanism must account for at least 10 (±5)% of the overall CH + CPD reaction mechanism to reproduce the measured 8% fulvene fraction.

6. CONCLUSIONS

Using PIMS-TOF product detection techniques, the direct formation of C_6H_6 isomers by the reaction of the methylidyne radical ($CH(X^2\prod)$) with cyclopentadiene has been observed. All C_6H_6 products observed in this work are formed through elimination of an H atom. Fitting the experimental photoion spectra to C_6H_6 reference spectra reveals that the two major products from the title reaction are benzene, with a branching fraction of 90 (±5)% and fulvene, with a branching fraction of 8 (±5)%. Several linear isomers are found to be minor products. The findings presented here suggest a novel and competitive route to benzene formation in combustion environments rich in cyclopentadiene.

Most studies of CH radicals reacting with unsaturated closed-shell hydrocarbons conclude that cycloaddition across a C=C bond dominates, with little evidence that CH inserts into C−H bonds.[47−50] In the present study, the experimental observation of fulvene strongly suggests that C−H insertion mechanisms play a non-negligible role compared to CH cycloaddition. It is therefore possible to conclude that the insertion mechanism accounts for at least 10 (±5)% of the overall CH + CPD mechanism to support the experimentally derived product branching fractions. Master Equation calculations that properly treat the competition between the barrierless CH + CPD entrance channels are substantially more difficult but would provide further information of the competitiveness of the insertion mechanisms relative to the cycloaddition mechanism. The experimental product branching fractions and mechanistic information are significant in exploring alternative and competitive routes to the formation benzene in carbon-rich gas phase environments.

■ ASSOCIATED CONTENT

Supporting Information

The Supporting Information is available free of charge at https://pubs.acs.org/doi/10.1021/acs.jpca.1c03517.

Absolute photoion spectra for C_6H_6 isomers, comparison of m/z 78 photoion spectra at 298 and 373 K, photoion spectra for m/z 64 and 65 along with reference fits, kinetic trace of m/z 27, mass spectra of CPD only and CPD + $CHBr_3$ over the m/z 35−150 range, branching fractions of C_6H_6 species for Figure 4a, m/z 78 photoion spectrum fit to benzene and fulvene only, m/z 78 and 79 photoion spectra for $CDBr_3$ + CPD, m/z 78 photoion spectra integrated over various kinetic times, expanded portion of the C_6H_7 PES, and the portion of the PES used in the MESMER calculations (PDF)

■ AUTHOR INFORMATION

Corresponding Author

Fabien Goulay − *C. Eugene Bennett Department of Chemistry, West Virginia University, Morgantown, West Virginia 26506, United States;* orcid.org/0000-0002-7807-1023; Email: Fabien.Goulay@mail.wvu.edu

https://doi.org/10.1021/acs.jpca.1c03517
J. Phys. Chem. A 2021, 125, 6927−6939

Authors

Kacee L. Caster − *C. Eugene Bennett Department of Chemistry, West Virginia University, Morgantown, West Virginia 26506, United States*

Talitha M. Selby − *Department of Mathematics and Natural Sciences, University of Wisconsin—Milwaukee, West Bend, Wisconsin 53095, United States*

David L. Osborn − *Combustion Research Facility, Sandia National Laboratories, Livermore, California 94551, United States;* orcid.org/0000-0003-4304-8218

Sebastien D. Le Picard − *IPR (Institut de Physique de Rennes), UMR 6251, Univ Rennes, CNRS, F-35000 Rennes, France*

Complete contact information is available at: https://pubs.acs.org/10.1021/acs.jpca.1c03517

Notes

The authors declare no competing financial interest.

■ ACKNOWLEDGMENTS

F.G. and K.L.C. are grateful to the National Science Foundation for its support of this work through Grant CHE-1764178. They also acknowledge travel support from the Eberly College of Art and Sciences and the C. Eugene Bennett Department of Chemistry at West Virginia University. The authors also thank the West Virginia University High Performance Computing shared facility for providing computing resources. T.M.S. thanks the Washington County Campus Foundation for financial support for this research. The Rennes team acknowledges support from the Agence Nationale de la Recherche, contract ANR-11-BS04-024-CRESUSOL-01, the French INSU/CNRS Program "Physique et Chimie du Milieu Interstellaire" (PCMI), the Institut Nationalde Physique (INPCNRS), the Région Bretagne, and the Université de Rennes 1. S.D.L.P. acknowledges financial support from the Institut Universitaire de France. The authors thank Raybel Almeida for technical support of this experiment. D.L.O. and the instrumentation for this work are supported by the Division of Chemical Sciences, Geosciences, and Biosciences, the Office of Basic Energy Sciences, the U.S. Department of Energy. Sandia National Laboratories is a multimission laboratory managed and operated by National Technology and Engineering Solutions of Sandia, LLC, a wholly owned subsidiary of Honeywell International, Inc. for the U.S. DOE's National Nuclear Security Administration under contract DE-NA0003525. This paper describes objective technical results and analysis. Any subjective views or opinions that might be expressed in the paper do not necessarily represent the views of the USDOE or the United States Government. This research used resources of the Advanced Light Source, a DOE Office of Science User Facility, which is supported by the Direct, Office of Science, Office of Basic Energy Sciences, the U.S. Department of Energy under contract DE-AC02-05CH11231 at Lawrence Berkeley National Laboratory.

■ REFERENCES

(1) Wilson, E. H.; et al. Mechanisms for the Formation of Benzene in the Atmosphere of Titan. *J. Geophys. Res.* **2003**, *108*, 1−10.

(2) Krasnopolsky, V. A. A Photochemical Model of Titan's Atmosphere and Ionosphere. *Icarus* **2009**, *201*, 226−256.

(3) Jones, B. M.; Zhang, F.; Kaiser, R. I.; Jamal, A.; Mebel, A. M.; Cordiner, M. A.; Charnley, S. B. Formation of Benzene in the Interstellar Medium. *Proc. Natl. Acad. Sci. U.S.A.* **2011**, *108*, 452−457.

(4) Woods, P. M.; Millar, T. J.; Zijlstra, A. A.; Herbst, E. The Synthesis of Benzene in the Proto−Planetary Nebula CRL 618. *Astrophys. J.* **2002**, *574*, L167−L170.

(5) Frenklach, M.; Feigelson, E. Formation of Polycyclic Aromatic Hydrocarbons in Circumstellar Envelopes. *Astrophys. J.* **1989**, *341*, 372−384.

(6) Kaiser, R. I.; Parker, D. S. N.; Mebel, A. M. Reaction Dynamics in Astrochemistry: Low-Temperature Pathways to Polycyclic Aromatic Hydrocarbons in the Interstellar Medium. *Annu. Rev. Phys. Chem.* **2015**, *66*, 43−67.

(7) Frenklach, M.; Mebel, A. On the Mechanism of Soot Formation. *Phys. Chem. Chem. Phys.* **2020**, *22*, 5314−5331.

(8) Cataldo, F. A Study of Soot Formed by Benzene Combustion. *Carbon* **1993**, *31*, 529−536.

(9) Richter, H.; Howard, J. B. Formation of Polycyclic Aromatic Hydrocarbons and Their Growth to Soot: A Review of Chemical Reaction Pathways. *Prog. Energy Combust. Sci.* **2000**, *26*, 565−608.

(10) Miller, J. A.; Klippenstein, S. J. The Recombination of Propargyl Radicals and Other Reactions on a C_6H_6 Potential Energy Surface. *J. Phys. Chem. A* **2003**, *107*, 7783−7799.

(11) Frenklach, M.; Clary, D. W.; Gardiner, W. C.; Stein, S. E. Detailed Kinetic Modeling of Soot Formation in Shock-Tube Pyrolysis of Acetylene. *Symp. (Int.) Combust.* **1985**, *20*, 887−901.

(12) Penney, W. G. The Theory of the Stability of the Benzene Ring and Related Compounds. *Proc. R. Soc. London, Ser. A* **1934**, *146*, 223−238.

(13) Wang, H. A.; Frenklach, M. A Detailed Kinetic Modeling Study of Aromatics Formation in Laminar Premixed Acetylene and Ethylene Flames. *Combust. Flame* **1997**, *110*, 173−221.

(14) Ruwe, L.; Moshammer, K.; Hansen, N.; Kohse-Höinghaus, K. Consumption and Hydrocarbon Growth Processes in a 2-Methyl-2-Butene Flame. *Combust. Flame* **2017**, *175*, 34−46.

(15) Johansson, K. O.; Head-Gordon, M. P.; Schrader, P. E.; Wilson, K. R.; Michelsen, H. A. Resonance-Stabilized Hydrocarbon-Radical Chain Reactions May Explain Soot Inception and Growth. *Science* **2018**, *361*, 997−1000.

(16) El Bakali, A.; Mercier, X.; Wartel, M.; Acevedo, F.; Burns, I.; Gasnot, L.; Pauwels, J. F.; Desgroux, P. Modeling of PAHs in Low Pressure Sooting Premixed Methane Flame. *Energy* **2012**, *43*, 73−84.

(17) Tielens, A. G. G. M. 25 Years of PAH Hypothesis. *EAS Publ. Ser.* **2011**, *46*, 3−10.

(18) Cherchneff, I. The Formation of Polycyclic Aromatic Hydrocarbons in Evolved Circumstellar Environments. *EAS Publ. Ser.* **2011**, *46*, 177−189.

(19) Woods, P. M. The Formation of Benzene in Dense Environments. *EAS Publ. Ser.* **2011**, *46*, 235−240.

(20) Bierbaum, V. M.; Le Page, V.; Snow, T. P. PAHs and the Chemistry of the ISM. *EAS Publ. Ser.* **2011**, *46*, 427−440.

(21) Hansen, N.; Schenk, M.; Moshammer, K.; Kohse-Höinghaus, K. Investigating Repetitive Reaction Pathways for the Formation of Polycyclic Aromatic Hydrocarbons in Combustion Processes. *Combust. Flame* **2017**, *180*, 250−261.

(22) Miller, J. A.; Klippenstein, S. J.; Georgievskii, Y.; Harding, L. B.; Allen, W. D.; Simmonett, A. C. Reactions between Resonance Stabilized Radicals: Propargyl + Allyl. *J. Phys. Chem. A* **2010**, *114*, 4881−4890.

(23) Miller, J. A.; Klippenstein, S. J. The Recombination of Propargyl Radicals: Solving the Master Equation. *J. Phys. Chem. A* **2001**, *105*, 7254−7266.

(24) Senosiain, J. P.; Miller, J. A. The Reaction of N- and i-C_4H_5 Radicals with Acetylene. *J. Phys. Chem. A* **2007**, *111*, 3740−3747.

(25) Krasnoukhov, V. S.; Porfiriev, D. P.; Zavershinskiy, I. P.; Azyazov, V. N.; Mebel, A. M. Kinetics of the CH_3 + C_5H_5 Reaction: A Theoretical Study. *J. Phys. Chem. A* **2017**, *121*, 9191−9200.

(26) Tang, W.; Tranter, R. S.; Brezinsky, K. Isomeric Product Distributions from the Self-Reaction of Propargyl Radicals. *J. Phys. Chem. A* **2005**, *109*, 6056−6065.

(27) Constantinidis, P.; Hirsch, F.; Fischer, I.; Dey, A.; Rijs, A. M. Products of the Propargyl Self-Reaction at High Temperatures

Investigated by IR/UV Ion Dip Spectroscopy. *J. Phys. Chem. A* **2017**, *121*, 181−191.
(28) Fahr, A.; Nayak, A. Kinetics and Products of Propargyl Radical Self-Reactions and Propargyl-Methyl Cross-Combination Reactions. *Int. J. Chem. Kinet.* **1999**, *32*, 118−124.
(29) Giri, B. R.; Hippler, H.; Olzmann, M.; Unterreiner, A. N. The Rate Coefficient of the C_3H_3 + C_3H_3 Reaction from UV Absorption Measurements after Photolysis of Dipropargyl Oxalate. *Phys. Chem. Chem. Phys.* **2003**, *5*, 4641−4646.
(30) Hansen, N.; Miller, J. A.; Kasper, T.; Kohse-Höinghaus, K.; Westmoreland, P. R.; Wang, J.; Cool, T. A. Benzene Formation in Premixed Fuel-Rich 1,3-Butadiene Flames. *Proc. Combust. Inst.* **2009**, *32*, 623−630.
(31) Georgievskii, Y.; Miller, J. A.; Klippenstein, S. J. Association Rate Constants for Reactions between Resonance-Stabilized Radicals: C_3H_3 + C_3H_3, C_3H_3 + C_3H_5, and C_3H_5 + C_3H_5. *Phys. Chem. Chem. Phys.* **2007**, *9*, 4259−4268.
(32) D'Anna, A.; Violi, A. Detailed Modeling of the Molecular Growth Process in Aromatic and Aliphatic Premixed Flames. *Energy Fuels* **2005**, *19*, 79−86.
(33) D'Anna, A.; Violi, A.; D'Alessio, A. Modeling the Rich Combustion of Aliphatic Hydrocarbons. *Combust. Flame* **2000**, *121*, 418−429.
(34) Howe, P. T.; Fahr, A. Pressure and Temperature Effects on Product Channels of the Propargyl ($HC{\equiv}CCH_2$) Combination Reaction and the Formation of the "First Ring. *J. Phys. Chem. A* **2003**, *107*, 9603−9610.
(35) Lockyear, J. F.; Fournier, M.; Sims, I. R.; Guillemin, J. C.; Taatjes, C. A.; Osborn, D. L.; Leone, S. R. Formation of Fulvene in the Reaction of C_2H with 1,3-Butadiene. *Int. J. Mass Spectrom.* **2015**, *378*, 232−245.
(36) Butler, J. E.; Fleming, J. W.; Goss, L. P.; Lin, M. C. Kinetics of CH Radical Reactions with Selected Molecules at Room Temperature. *Chem. Phys.* **1981**, *56*, 355−365.
(37) Butler, J. E.; Fleming, J. W.; Goss, L. P.; Lin, M. C. Kinetics of CH Radical Reactions Important to Hydrocarbon Combustion Systems. *Laser Probes for Combustion Chemistry*; ACS Publications, 1980; Chapter 33, pp 397−401.
(38) Canosa, A.; Sims, I. R.; Travers, D.; Smith, I. W. M.; Rowe, B. R. Reactions of the Methylidine Radical with CH_4, C_2H_2, C_2H_4, C_2H_6, and but-1-Ene Studied between 23 and 295 K with a CRESU Apparatus. *Astron. Astrophys.* **1997**, *323*, 644−651.
(39) Zabarnick, S.; Fleming, J. W.; Lin, M. C. Kinetics of $CH(X^2\Pi)$ Radical Reactions with Cyclopropane, Cyclopentane, and Cyclohexane. *J. Chem. Phys.* **1988**, *88*, 5983−5984.
(40) Berman, M. R.; Fleming, J. W.; Harvey, A. B.; Lin, M. C. Temperature Dependence of the Reactions of CH Radicals with Unsaturated Hydrocarbons. *Chem. Phys.* **1982**, *73*, 27−33.
(41) Zou, P.; Shu, J.; Sears, T. J.; Hall, G. E.; North, S. W. Photodissociation of Bromoform at 248 nm: Single and Multiphoton Processes. *J. Phys. Chem. A* **2004**, *108*, 1482−1488.
(42) Hodgkinson, G. J. Interstellar Chemistry. *J. Br. Astron. Assoc.* **1979**, *89*, 331−355.
(43) Blitz, M. A.; Seakins, P. W. Laboratory Studies of Photochemistry and Gas Phase Radical Reaction Kinetics Relevant to Planetary Atmospheres. *Chem. Soc. Rev.* **2012**, *41*, 6318−6347.
(44) Luque, J.; Berg, P. A.; Jeffries, J. B.; Smith, G. P.; Crosley, D. R.; Scherer, J. J. Cavity Ring-down Absorption and Laser-Induced Fluorescence for Quantitative Measurements of CH Radicals in Low-Pressure Flames. *Appl. Phys. B: Lasers Opt.* **2004**, *78*, 93−102.
(45) Blevins, L. G.; Renfro, M. W.; Lyle, K. H.; Laurendeau, N. M.; Gore, J. P. Experimental Study of Temperature and CH Radical Location in Partially Premixed CH_4/Air Coflow Flames. *Combust. Flame* **1999**, *118*, 684−696.
(46) Schofield, K.; Steinberg, M. CH and C_2 Measurements Imply a Radical Pool within a Pool in Acetylene Flames. *J. Phys. Chem. A* **2007**, *111*, 2098−2114.
(47) Goulay, F.; Trevitt, A. J.; Meloni, G.; Selby, T. M.; Osborn, D. L.; Taatjes, C. A.; Vereecken, L.; Leone, S. R. Cyclic versus Linear Isomers Produced by Reaction of the Methylidyne Radical (CH) with Small Unsaturated Hydrocarbons. *J. Am. Chem. Soc.* **2009**, *131*, 993−1005.
(48) Goulay, F.; Trevitt, A. J.; Savee, J. D.; Bouwman, J.; Osborn, D. L.; Taatjes, C. A.; Wilson, K. R.; Leone, S. R. Product Detection of the CH Radical Reaction with Acetaldehyde. *J. Phys. Chem. A* **2012**, *116*, 6091−6106.
(49) Goulay, F.; Derakhshan, A.; Maher, E.; Trevitt, A. J.; Savee, J. D.; Scheer, A. M.; Osborn, D. L.; Taatjes, C. A. Formation of Dimethylketene and Methacrolein by Reaction of the CH Radical with Acetone. *Phys. Chem. Chem. Phys.* **2013**, *15*, 4049−4058.
(50) Trevitt, A. J.; Goulay, F. Insights into Gas-Phase Reaction Mechanisms of Small Carbon Radicals Using Isomer-Resolved Product Detection. *Phys. Chem. Chem. Phys.* **2016**, *18*, 5867−5882.
(51) Maksyutenko, P.; Zhang, F.; Gu, X.; Kaiser, R. I. A Crossed Molecular Beam Study on the Reaction of Methylidyne Radicals [$CH(X^2\Pi)$] with Acetylene [C_2H_2 ($X^1\sum_g^+$)]—Competing C_3H_2 + H and C_3H + H. *Phys. Chem. Chem. Phys.* **2011**, *13*, 240−252.
(52) Goulay, F.; Trevitt, A. J.; Savee, J. D.; Bouwman, J.; Osborn, D. L.; Taatjes, C. A.; Wilson, K. R.; Leone, S. R. Product Detection of the CH Radical Reaction with Acetaldehyde. *J. Phys. Chem. A* **2012**, *116*, 6091−6106.
(53) Carrasco, E.; Meloni, G. Study of Methylidyne Radical (CH and CD) Reaction with 2,5-Dimethylfuran Using Multiplexed Synchrotron Photoionization Mass Spectrometry. *J. Phys. Chem. A* **2018**, *122*, 6118−6133.
(54) Carrasco, E.; Smith, K. J.; Meloni, G. Synchrotron Photoionization Study of Furan and 2-Methylfuran Reactions with Methylidyne Radical (CH) at 298 K. *J. Phys. Chem. A* **2018**, *122*, 280−291.
(55) Soorkia, S.; Taatjes, C. A.; Osborn, D. L.; Selby, T. M.; Trevitt, A. J.; Wilson, K. R.; Leone, S. R. Direct Detection of Pyridine Formation by the Reaction of CH (CD) with Pyrrole: A Ring Expansion Reaction. *Phys. Chem. Chem. Phys.* **2010**, *12*, 8750−8758.
(56) Herbinet, O.; Rodriguez, A.; Husson, B.; Battin-Leclerc, F.; Wang, Z.; Cheng, Z.; Qi, F. Study of the Formation of the First Aromatic Rings in the Pyrolysis of Cyclopentene. *J. Phys. Chem. A* **2016**, *120*, 668−682.
(57) Butler, R. G.; Glassman, I. Cyclopentadiene Combustion in a Plug Flow Reactor near 1150 K. *Proc. Combust. Inst.* **2009**, *32*, 395−402.
(58) Djokic, M. R.; Van Geem, K. M.; Cavallotti, C.; Frassoldati, A.; Ranzi, E.; Marin, G. B. An Experimental and Kinetic Modeling Study of Cyclopentadiene Pyrolysis: First Growth of Polycyclic Aromatic Hydrocarbons. *Combust. Flame* **2014**, *161*, 2739−2751.
(59) Cavallotti, C.; Polino, D.; Frassoldati, A.; Ranzi, E. Analysis of Some Reaction Pathways Active during Cyclopentadiene Pyrolysis. *J. Phys. Chem. A* **2012**, *116*, 3313−3324.
(60) Vervust, A. J.; Djokic, M. R.; Merchant, S. S.; Carstensen, H.; Long, A. E.; Marin, G. B.; Green, W. H.; Van Geem, K. M. Detailed Experimental and Kinetic Modeling Study of Cyclopentadiene Pyrolysis in the Presence of Ethene. *Energy Fuels* **2018**, *32*, 3920−3934.
(61) Caster, K. L.; Donnellan, Z. N.; Selby, T. M.; Goulay, F. Kinetic Investigations of the $CH(X^2\Pi)$ Radical Reaction with Cyclopentadiene. *J. Phys. Chem. A* **2019**, *123*, 5692−5703.
(62) Lockyear, J. F.; Welz, O.; Savee, J. D.; Goulay, F.; Trevitt, A. J.; Taatjes, C. A.; Osborn, D. L.; Leone, S. R. Isomer Specific Product Detection in the Reaction of CH with Acrolein. *J. Phys. Chem. A* **2013**, *117*, 11013−11026.
(63) Glowacki, D. R.; Liang, C. H.; Morley, C.; Pilling, M. J.; Robertson, S. H. MESMER: An Open-Source Master Equation Solver for Multi-Energy Well Reactions. *J. Phys. Chem. A* **2012**, *116*, 9545−9560.
(64) Osborn, D. L.; Zou, P.; Johnsen, H.; Hayden, C. C.; Taatjes, C. A.; Knyazev, V. D.; North, S. W.; Peterka, D. S.; Ahmed, M.; Leone, S. R. The Multiplexed Chemical Kinetic Photoionization Mass Spectrometer: A New Approach to Isomer-Resolved Chemical Kinetics. *Rev. Sci. Instrum.* **2008**, *79*, No. 104103.

https://doi.org/10.1021/acs.jpca.1c03517
J. Phys. Chem. A 2021, 125, 6927−6939

(65) Taatjes, C. A.; Hansen, N.; Osborn, D. L.; Kohse-Höinghaus, K.; Cool, T. A.; Westmoreland, P. R. "Imaging"' Combustion Chemistry via Multiplexed Synchrotron-Photoionization Mass Spectrometry. *Phys. Chem. Chem. Phys.* **2008**, *10*, 20−34.
(66) Herbert, L. B.; Sims, I. R.; Smith, I. W. M.; Stewart, D. W. A.; Symonds, A. C.; Canosa, A.; Rowe, B. R. Rate Constants for the Relaxation of $CH(X^2\Pi)$ by CO and N_2 at Temperatures from 23 to 584 K. *J. Phys. Chem. A* **1996**, *100*, 14928−14935.
(67) Romanzin, C.; Boyé-Péronne, S.; Gauyacq, D.; Bénilan, Y.; Gazeau, M. C.; Douin, S. CH Radical Production from 248 Nm Photolysis or Discharge-Jet Dissociation of CHBr3 Probed by Cavity Ring-down Absorption Spectroscopy. *J. Chem. Phys.* **2006**, *125*, No. 114312.
(68) Moffett, R. B. Cyclopentadiene and 3-Chlorocyclopentene. *Org. Synth.* **1952**, *32*, 41−44.
(69) Montgomery, J. A.; Frisch, M. J.; Ochterski, J. W.; Petersson, G. A. A Complete Basis Set Model Chemistry. VII. Use of Density Functional Geometries and Frequencies. *J. Chem. Phys.* **1999**, *110*, 2822−2827.
(70) Frisch, M. J.; Trucks, G. W.; Schlegel, H. B.; Scuseria, G. E.; Robb, M. A.; Cheeseman, J. R.; Scalmani, G. *Gaussian 09*; Gaussian, Inc.: Wallingford, CT, 2016.
(71) Becke, A. D. A New Mixing of Hartree-Fock and Local Density-Functional Theories. *J. Chem. Phys.* **1993**, *98*, 1372−1377.
(72) Ervin, K. M. *Fortran Program PESCAL*; University of Nevada: Reno, 2004.
(73) Bobeldijk, M.; van der Zande, W. J.; Kistemaker, P. G. Simple Models for the Calculation of Photoionization and Electron Impact Ionization Cross Sections of Polyatomic Molecules. *Chem. Phys.* **1994**, *179*, 125−130.
(74) Blitz, M. A.; Talbi, D.; Seakins, P. W.; Smith, I. W. M. Rate Constants and Branching Ratios for the Reaction of CH Radicals with NH_3: A Combined Experimental and Theoretical Study. *J. Phys. Chem. A* **2012**, *116*, 5877−5885.
(75) Shannon, R. J.; Caravan, R. L.; Blitz, M. A.; Heard, D. E. A Combined Experimental and Theoretical Study of Reactions between the Hydroxyl Radical and Oxygenated Hydrocarbons Relevant to Astrochemical Environments. *Phys. Chem. Chem. Phys.* **2014**, *16*, 3466−3478.
(76) Pakhira, S.; Lengeling, B. S.; Olatunji-Ojo, O.; Caffarel, M.; Frenklach, M.; Lester, W. A. A Quantum Monte Carlo Study of the Reactions of CH with Acrolein. *J. Phys. Chem. A* **2015**, *119*, 4214−4223.
(77) Cool, T. A.; Wang, J.; Nakajima, K.; Taatjes, C. A.; Mcllroy, A. Photoionization Cross Sections for Reaction Intermediates in Hydrocarbon Combustion. *Int. J. Mass Spectrom.* **2005**, *247*, 18−27.
(78) Powell, J. S.; Edson, K. C. Spectroscopic Determination of Cyclopentadiene and Methylcyclopentadiene. *Anal. Chem.* **1948**, *20*, 510−511.
(79) Yu, L.; Foster, S. C.; Williamson, J. M.; Heaven, M. C.; Miller, T. A. Rotationally Resolved Electronic Spectrum of Jet-Cooled Cyclopentadienyl Radical. *J. Phys. Chem. A* **1988**, *92*, 4263−4266.
(80) Savee, J. D.; Selby, T. M.; Welz, O.; Taatjes, C. A.; Osborn, D. L. Time- and Isomer-Resolved Measurements of Sequential Addition of Acetylene to the Propargyl Radical. *J. Phys. Chem. Lett.* **2015**, *6*, 4153−4158.
(81) Hansen, N.; Klippenstein, S. J.; Miller, J. A.; Wang, J.; Cool, T. A.; Law, M. E.; Westmoreland, P. R.; Kasper, T.; Kohse-Höinghaus, K. Identification of C_5H_x Isomers in Fuel-Rich Flames by Photoionization Mass Spectrometry and Electronic Structure Calculations. *J. Phys. Chem. A* **2006**, *110*, 4376−4388.
(82) Goulay, F.; Osborn, D. L.; Taatjes, C. A.; Zou, P.; Meloni, G.; Leone, S. R. Direct Detection of Polyynes Formation from the Reaction of Ethynyl Radical (C_2H) with Propyne (CH_3-C≡CH) and Allene (CH_2=C=CH_2). *Phys. Chem. Chem. Phys.* **2007**, *9*, 4291−4300.
(83) Shapero, M.; Ramphal, I. A.; Neumark, D. M. Photodissociation of the Cyclopentadienyl Radical at 248-Nm. *J. Phys. Chem. A* **2018**, *122*, 4265−4272.
(84) Knyazev, V. D.; Popov, K. V. Kinetics of the Self Reaction of Cyclopentadienyl Radicals. *J. Phys. Chem. A* **2015**, *119*, 7418−7429.
(85) Savee, J. D.; Soorkia, S.; Welz, O.; Selby, T. M.; Taatjes, C. A.; Osborn, D. L. Absolute Photoionization Cross-Section of the Propargyl Radical. *J. Chem. Phys.* **2012**, *136*, No. 134307.
(86) Savee, J. D.; Lockyear, J. F.; Borkar, S.; Eskola, A. J.; Welz, O.; Taatjes, C. A.; Osborn, D. L. Note: Absolute Photoionization Cross-Section of the Vinyl Radical. *J. Chem. Phys.* **2013**, *139*, No. 056101.
(87) Chikan, V.; Fournier, F.; Leone, S. R.; Nizamov, B. State-Resolved Dynamics of the $CH(A^2\Delta)$ Channels from Single and Multiple Photon Dissociation of Bromoform in the 10-20 EV Energy Range. *J. Phys. Chem. A* **2006**, *110*, 2850−2857.
(88) Zou, P.; Shu, J.; Sears, T. J.; Hall, G. E.; North, S. W. Photodissociation of Bromoform at 248 Nm: Single and Multiphoton Processes. *J. Phys. Chem. A* **2004**, *108*, 1482−1488.
(89) Soorkia, S.; Trevitt, A. J.; Selby, T. M.; Osborn, D. L.; Taatjes, C. A.; Wilson, K. R.; Leone, S. R. Reaction of the C_2H Radical with 1-Butyne (C_4H_6): Low-Temperature Kinetics and Isomer-Specific Product Detection. *J. Phys. Chem. A* **2010**, *114*, 3340−3354.
(90) Jasper, A. W.; Hansen, N. Hydrogen-Assisted Isomerizations of Fulvene to Benzene and of Larger Cyclic Aromatic Hydrocarbons. *Proc. Combust. Inst.* **2013**, *34*, 279−287.
(91) Melius, C.; Colvin, M.; Marinov, N.; Pitz, W.; Senkan, S. Reaction Mechanisms in Aromatic Hydrocarbon Formation Involving the C_5H_5 Cyclopentadienyl Moiety. *Symp. (Int.) Combust.* **1996**, *26*, 685−692.
(92) Miller, J. A.; Klippenstein, S. J. The Recombination of Propargyl Radicals: Solving the Master Equation. *J. Phys. Chem. A* **2001**, *105*, 7254−7266.
(93) Soorkia, S.; Taatjes, C. A.; Osborn, D. L.; Selby, T. M.; Trevitt, A. J.; Wilson, K. R.; Leone, S. R. Direct Detection of Pyridine Formation by the Reaction of CH (CD) with Pyrrole: A Ring Expansion Reaction. *Phys. Chem. Chem. Phys.* **2010**, *12*, 8750−8758.
(94) Sharma, S.; Green, W. H. Computed Rate Coefficients and Product Yields for C_5H_5 + CH_3. *J. Phys. Chem. A* **2009**, *113*, 8871−8882.
(95) Ribeiro, J. M.; Mebel, A. M. Reaction Mechanism and Product Branching Ratios of the CH + C_3H_6 Reaction: A Theoretical Study. *J. Phys. Chem. A* **2016**, *120*, 1800−1812.
(96) Ribeiro, J. M.; Mebel, A. M. Reaction Mechanism and Product Branching Ratios of the CH + C_3H_8 Reaction: A Theoretical Study. *J. Phys. Chem. A* **2014**, *118*, 9080−9086.
(97) Galland, N.; Caralp, F.; Hannachi, Y.; Bergeat, A.; Loison, J. C. Experimental and Theoretical Studies of the Methylidyne Radical Reaction with Ethane (C_2H_6): Overall Rate Constant and Product Channels. *J. Phys. Chem. A* **2003**, *107*, 5419−5426.
(98) Loison, J.-C.; Bergeat, A. Rate Constants and the H Atom Branching Ratio of the Reactions of the Methylidyne $CH(X^2\Pi)$ Radical with C_2H_2, C_2H_4, C_3H_4, C_3H_6 and C_4H_8. *Phys. Chem. Chem. Phys.* **2009**, *11*, 655−664.

https://doi.org/10.1021/acs.jpca.1c03517
J. Phys. Chem. A 2021, 125, 6927−6939